Center-Surround Interactions in the Middle Temporal Visual Area of the Owl Monkey

RICHARD T. BORN
Department of Neurobiology, Harvard Medical School, Boston, Massachusetts 02115-5701

Received 7 December 1999; accepted in final form 6 July 2000

Born, Richard T. Center-surround interactions in the middle temporal visual area of the owl monkey. *J Neurophysiol* 84: 2658–2669, 2000. Microelectrode recording and 2-deoxyglucose (2dg) labeling were used to investigate center-surround interactions in the middle temporal visual area (MT) of the owl monkey. These techniques revealed columnar groups of neurons whose receptive fields had opposite types of center-surround interaction with respect to moving visual stimuli. In one type of column, neurons responded well to objects such as a single bar or spot but poorly to large textured stimuli such as random dots. This was often due to the fact that the receptive fields had *antagonistic* surrounds: surround motion in the same direction as that preferred by the center suppressed responses, thus rendering these neurons unresponsive to wide-field motion. In the second set of complementary, interdigitated columns, neuronal receptive fields had *reinforcing* surrounds and responded optimally to wide-field motion. This functional organization could not be accounted for by systematic differences in binocular disparity. Within both column types, neurons whose receptive fields exhibited center-surround interactions were found less frequently in the input layers compared with the other layers. Additional tests were done on single units to examine the nature of the center-surround interactions. The direction tuning of the surround was broader than that of the center, and the preferred direction, with respect to that of the center, tended to be either in the *same* or *opposite* direction and only rarely in orthogonal directions. Surround motion at various velocities modulated the overall responsiveness to centrally placed moving stimuli, but it did not produce shifts in the peaks of the center's tuning curves for either direction or speed. In layers 3B and 5 of the local motion processing columns, a number of neurons responded only to local motion contrast but did so over a region of the visual field that was much larger than the optimal stimulus size. The central feature of this receptive field type was the *generalization* of surround antagonism over retinotopic space—a property similar to other "complex" receptive fields described previously. The columnar organization of different types of center-surround interactions may reflect the initial segregation of visual motion information into wide-field and local motion contrast systems that serve complementary functions in visual motion processing. Such segregation appears to occur at later stages of the macaque motion processing stream, in the medial superior temporal area (MST), and has also been described in invertebrate visual systems where it appears to be involved in the important function of distinguishing background motion from object motion.

INTRODUCTION

Center-surround interactions play an important role in processing sensory information (Allman et al. 1985b). By allowing a neuron to make a comparison between activity in a restricted set of "central" inputs and those in the area immediately adjacent, the interactions can make explicit even subtle *changes* in the representation across the input layer. Since spatial variation is a key feature of objects of interest to an organism, the center-surround operator is a very effective means of refining sensory representations and rendering them more efficient (Attneave 1954; Grossberg 1983; Nakayama and Loomis 1974).

Examples of center-surround receptive field organization can be found in nearly every sensory domain that has been studied, including vision (Barlow 1953; Hartline 1940; Kuffler 1953; Maturana et al. 1960), audition (Knudsen and Konishi 1978), touch (Mountcastle and Powell 1959), olfaction (Yokoi et al. 1995), and electroreception (Bastian 1974). Center-surround organization is particularly prominent in the visual system, where it is encountered as early as retinal bipolar cells (Kaneko 1970; Werblin and Dowling 1969) and at least as late as extrastriate visual areas such as V4, where it appears to be involved in comparisons used for processing both form (Desimone and Schein 1987) and color (Schein and Desimone 1990), and the middle temporal visual area (MT) (Allman et al. 1985a) and MSTl (Eifuku and Wurtz 1998), where it is presumably involved in motion processing.

In motion processing areas, the center-surround organization of the receptive fields yields interesting properties. Some neurons respond to a short bar of light or a small patch of random dots moving in their preferred direction, but this response is suppressed as the stimulus is made larger. In some cases, the response to a small, centrally located stimulus can be enhanced by opposing motion in the area surrounding the so-called "classical receptive field" (CRF). This property has been found in MT neurons in both the owl monkey (Allman et al. 1985a) and the macaque (Lagae et al. 1989; Tanaka et al. 1986) as well as in cat superior colliculus (Sterling and Wickelgren 1969) and lateral suprasylvian area (von Grunau and Frost 1983), and in pigeon optic tectum (Frost and Nakayama 1983; Frost et al. 1981). The antagonistic surrounds of these neurons render them insensitive to wide-field motion but sensitive to local motion *contrast*. Other types of motion-sensitive neurons have surrounds that reinforce the center—i.e., the surround's direction preference is similar to that of the center—the result of

Address for reprint requests: Dept. of Neurobiology, Harvard Medical School, 220 Longwood Ave., Boston, MA 02115-5701 (E-mail: rborn@hms.harvard.edu).

The costs of publication of this article were defrayed in part by the payment of page charges. The article must therefore be hereby marked "*advertisement*" in accordance with 18 U.S.C. Section 1734 solely to indicate this fact.

which is that they respond best to wide-field motion (Allman et al. 1985a; Tanaka et al. 1986).

That these two different types of neurons are segregated from each other within MT of the owl monkey was indicated by 2-deoxyglucose (2dg) experiments and microelectrode recordings (Born and Tootell 1992). A wide-field random dot stimulus moving coherently at systematically varied directions, speeds, and binocular disparities produced patchy regions of high 2dg uptake, termed "bands," and intervening low-uptake regions, called "interbands." Microelectrode penetrations showed that the center-surround properties of neurons in MT were also clustered and that they appeared to correspond to the 2dg patterns. Furthermore, the center-surround properties were similar within a given penetration perpendicular to the cortical surface, suggesting a columnar organization.

In the present study, the relationships between the 2dg band-interband patterns and single-unit properties are explored in greater quantitative detail, and further evidence for a columnar organization is presented. Additionally, the nature of the center-surround relationships—with respect to tuning for both direction and speed, and with respect to positional invariance—are examined. These experiments show evidence for further hierarchical processing of motion cues within a column.

METHODS

Surgical preparation

All procedures were approved by the Harvard Medical Area Standing Committee on Animals. One week prior to the experiment, an owl monkey (*Aotus nancymai)* was anesthetized with pentobarbital sodium, and, under sterile conditions, a dental acrylic head post was attached to its skull. On the day of an experiment, anesthesia was induced with ketamine (15 mg/kg im), the animal was intubated, an intravenous catheter was inserted, electrocardiographic (EKG) leads attached, and a blood pressure cuff placed around the arm. Core body temperature was monitored with a rectal temperature probe and maintained at 37.5°C by a thermostat-controlled heating pad. End-tidal pCO_2 was continuously monitored and maintained within physiological limits during electrophysiological recording. After a loading dose of sufentanil (7.20 μg/kg iv), anesthesia was maintained with a constant intravenous infusion of sufentanil (2–8 $\mu g \cdot kg^{-1} \cdot h^{-1}$). Adequacy of anesthesia was ensured by monitoring EKG and blood pressure and supplementing the constant infusion with an intravenous bolus of sufentanil (1 μg/kg) if either measure increased 10% or more above baseline in response to a pinch of the tail or a nail bed. For more rapid control of anesthetic levels, we often supplemented the sufentanil with a small amount of isoflurane (0.25–0.5% in oxygen). In tests on unparalyzed animals, these measures were sensitive and early indicators of lightened anesthesia, preceding by several minutes any movement by the animal in response to painful stimuli.

All incision sites were first thoroughly infiltrated with a long-acting local anesthetic (0.5% bupivicaine with 1:200,000 epinephrine). A small craniotomy (approximately 2 mm diam) was made with a high-speed dental drill, after which the underlying dura was bluntly dissected using fine forceps. After surgical procedures were completed, the animal was paralyzed with a continuous intravenous infusion of a combination of gallamine triethiodide (10 $mg \cdot kg^{-1} \cdot h^{-1}$) and curare (0.1 $mg \cdot kg^{-1} \cdot h^{-1}$).

Optics

After topical infusion of a local anesthetic (proparacaine HCl, 0.5%), corneal curvature was measured with a keratometer, and gas-permeable contact lenses of the appropriate basal curvature were placed over the eyes. The pupils were dilated and accommodation paralyzed with atropine eye drops. The eyes were refracted for the appropriate distance, usually 57 cm, using trial lenses, and a Risley prism was placed over the right eye so that receptive fields from the two eyes could be brought into register.

Stimulus generation and data acquisition

Stimuli were generated by a Silicon Graphics IRIS 3130 computer and displayed on a Sony Trinitron color monitor with resolution of 1,024 × 786 pixels at a 60-Hz noninterlaced refresh rate. Stimuli could be controlled either manually, using a mouse and a "dial-and-button" box, or by a second computer via a serial port interface. This second computer also collected and stored the unit data using a counter-timer board (Metrabyte CTM05).

Neuronal signals were recorded using glass-coated tungsten microelectrodes (Merrill and Ainsworth 1972) with standard amplification and filtering. Single units were isolated on the basis of constant spike height and waveform. When a unit was encountered that could be clearly discriminated from the background activity, it was studied using a variety of stimuli including bars, spots, annuli, gratings, and random dots. It was attempted to resolve single units approximately every 100 μm to obtain adequate spatial sampling. In situations where this was not possible, multi-unit activity was recorded.

Once the location of the receptive field was found, its borders were mapped with a light bar using the minimal response technique (Barlow et al. 1967). This region will be subsequently referred to as the CRF. The optimal direction, speed, and binocular disparity were determined qualitatively by listening to the spike output on a loudspeaker. In all subsequent tests, these qualitatively optimized parameters were used and held constant from trial to trial. If the neuron responded as well to stimuli presented to one eye as it did to any combination of the two eyes (determined by adjusting the Risley prism while listening to the cell's spike output), it was tested monocularly. In cases where the neuron responded well only to binocular stimuli at a particular disparity, the best disparity was used for subsequent testing. The neuron's optimal stimulus (random dots vs. a single bar), and the overall response to a large field of random dots were also recorded.

Quantitative tests

Quantitative data were collected using a personal computer (PC) to coordinate stimulus presentation and record spike arrival times in the form of peristimulus time histograms (PSTHs). Data were analyzed and displayed graphically on-line showing the unit's response before, during, and after stimulus presentation as a function of a given stimulus parameter value. Stimuli were presented in a blockwise random order with a minimum of five repetitions of each stimulus.

Two basic measures of center-surround interactions were used: an area summation test (Fig. 1*A*) in which the response of the cell was measured as a function of the aperture size of a circular patch of moving random dots (dot density constant) centered in the CRF, and the surround direction test (Fig. 1*B*), which involved sweeping an optimally oriented bar (constant on all trials) across the center of the CRF while the direction of motion of a large surround annulus of random dots was varied from trial to trial. The area summation curve (ASC) provided information on the size, strength, and polarity of the surround. The surround direction test was an important supplement to the area summation test since many interband neurons did not respond well even to small patches of random dots but did respond well to bars.

Data analysis

Area summation test data were analyzed in two ways. First, the slope of the regression line was used a measure of the strength of

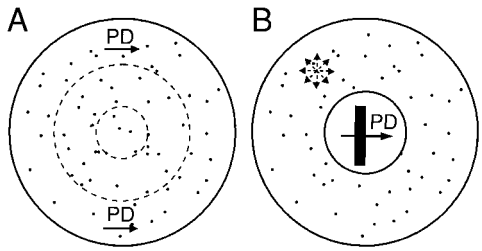

FIG. 1. Visual stimuli used for quantitative testing of neurons. *A*: area summation test. The neuron was tested with random dot patterns moving within circular windows of varying diameters. The dots always moved in the neuron's preferred direction and speed, and, if necessary, at an optimal binocular disparity. *B*: surround direction tuning. The center of the neuron's receptive field was stimulated on all trials with a single bar that moved in the preferred direction (PD) and speed. The surround was stimulated with an annular window of random dots whose direction of motion varied from trial to trial. In addition, 2 control conditions were included: 1 in which only the center stimulus moved while the surround stimulus was on but remained stationary and 1 in which only the surround stimulus moved while the center stimulus remained stationary. In both of these control conditions, the direction used was the preferred direction of the center.

surround antagonism (SA). For curves that showed a rising limb before a falling limb (e.g., Fig. 6*A*), the regression line was fit to the falling limb. This was only done when it was clear that suppression was the dominant effect of the surround and, in nearly all cases, simply meant excluding the first point (smallest aperture size) from the regression. Each neuron was also classified as having either "strong," "weak," or "no" SA. Cells from which area summation data were obtained were classified according to the slope of the regression line fit to this data: strong SA, slope less than -0.03; weak SA, $-0.03 \leq$ slope < 0; and no SA, slope ≥ 0 or not significantly different from 0. At sites where quantitative area summation data were not obtained, cells were classified based on a qualitative comparison of the response to wide-field stimuli, such as large random dot patches and gratings and small, discrete stimuli, such as bars and spots. As a second measure of center-surround interaction, a surround index (SI) was calculated to compare the response to small field (SF) and wide-field (WF) motion: $(WF - SF)/(WF + SF)$. Values approaching -1 indicated strong SA; values approaching $+1$ indicated strong area summation. Surround direction test data were fit with a Gaussian having four free parameters: amplitude, offset, mean and standard deviation. The mean and standard deviation parameters were used as a measure of the direction preference and the tuning bandwidth [full width at half height = 2.36*sigma (Carney and Shadlen 1993)], respectively.

Histological reconstructions

During each electrode penetration, from two to five lesions were made by passing current through the electrode tip (1.5–2.5 μA for 1–2 s, electrode negative) to serve as markers for subsequent track reconstructions. The standard practice was to locate a recording site at which to make a lesion, record cells beyond this for 150–250 μm, and then back up to make the lesion. Five to 10 min after backing up to the site, the unit properties were reconfirmed prior to making the lesion. This technique was a compromise designed to prevent large gaps in data collection around the lesion while still permitting precise correspondence between the physical lesions and the microdrive readings.

2dg

For four of the oblique penetrations, at the end of the physiology recording the band-interband patterns were labeled with 2dg (Kennedy et al. 1975; Tootell et al. 1988). The stimulus monitor was moved in to 28.5 cm, and the animal's eyes were again refracted before inserting a recording electrode into striate cortex. A perifoveal, binocular single unit was then isolated to align the eyes using the Risley prism.

Ten minutes prior to infusion of the 2dg, the animal was given an injection of methamphetamine (50 μg/kg im) while heart rate, blood pressure, and cortical activity were monitored to ensure that the level of anesthesia remained adequate. An increased level of catecholamines has been reported to sharpen cortical columns labeled by 2dg (Craik et al. 1987). Subsequent experiments in four animals showed that this dose of methamphetamine did not qualitatively affect the patterns—compare the 2dg pattern in Fig. 6 (obtained *with* methamphetamine) with those in Fig. 7 (obtained *without* methamphetamine)—although it did tend to improve the contrast. During infusion of the 2dg, the animal viewed a large field of random dots that moved in systematically varied directions (15° increments) and speeds (10, 15, 25°/s) over the 45 min of the experiment. In some experiments, the density of the random dot display (0.5, 1, and 2%) and the binocular disparity ($\pm$2 diopters) were also varied, but neither manipulation affected the patterns so obtained. The 2dg (50–200 μCi/kg; 2-[1–14C]deoxyglucose; American Radiolabeled Chemical, St. Louis, MO) was infused slowly over the first 10 min to avoid bias in uptake caused by any single stimulus condition. After 45 min, the animal was deeply anesthetized with pentobarbital sodium (50 mg/kg iv) followed by intracardial perfusion and fixation (0.9% NaCl, 13% sucrose followed by 2.5% glutaraldehyde/0.7% formaldehyde in 0.1 M PB, pH = 7.4 also with 13% sucrose). The brain was quickly removed from the cranium, the cortical sulci were unfolded and each hemisphere was flattened and then immediately frozen on a glass slide placed on top of a metal block that had been cooled with dry ice (Tootell and Silverman 1985).

Sections were cut on a cryostat (Frigocut 8000; 40 μm) parallel to the cortical surface and placed on subbed coverslips. The coverslips were glued to 20 $\times$ 25 cm sheets of cardboard, then apposed to X-ray film (Kodak MinR) for periods of 1–6 wk, depending on the amount of isotope infused. Once satisfactory autoradiographs were obtained, alternate sections were processed for cytochrome oxidase (CO) (Wong-Riley 1979) or Nissl substance or both.

For perpendicular microelectrode penetrations, 2dg labeling was not performed because earlier experiments had shown that the craniotomy overlying the electrode track caused intense, artifactual 2dg uptake that obscured any patterns that might have been present. On completion of the unit recording, the animal was perfused, under deep barbiturate anesthesia, with 1 l of 0.9% NaCl followed by 2–3 l of 2.5% glutaraldehyde and 0.7% formaldehyde in 0.1 M PB (pH 7.4). The brain was removed from the skull, and the tissue was blocked in the coronal plane and dropped into a chilled solution of 15% sucrose in 0.1 M PB. This was kept on a shaker tray at 4°C for 1–2 days then transferred to a 30% sucrose solution for another 2–3 days. After this, 60- to 80-μm-thick sections were cut in the coronal plane on a freezing sliding microtome, mounted onto subbed glass slides, and stained with cresyl violet.

Electrode track reconstructions

For perpendicular penetrations, the section containing the lesions was photographed through a microscope (Zeiss Axioskop) using brightfield illumination. Laminar boundaries were located on the photograph and their location relative to the lesions was used to assign each boundary a number in electrode track coordinates. In this way, each recording site was assigned to one of seven specific layers: 1 (from which no data were recorded), 2/3A, 3B (distinguished by the presence of large pyramidal cells), 4 (granular cortex), 5, and 6A [arbitrarily defined as the first 50 μm of layer 6, which also receives inputs from V1 (Rockland 1989)] and 6B.

For oblique penetrations, the electrode track reconstructions were somewhat more involved because the tissue was sectioned parallel to the surface of the flattened cortex. The lesions were first located on different CO sections. These sections were scanned into an image

processor so that subsequent images could be aligned using the patterns of radially penetrating blood vessels as guides. The horizontal progress of the electrode track was charted from section to section, and each successive section was kept in register within the computer's memory. The reconstructed track was superimposed on the 2dg patterns that had been scanned in at the same magnification, again using blood vessels and tissue artifacts as guides for alignment. Using the distances between lesions and the corresponding microdrive readings for the lesion sites, a scaling factor was computed, which then allowed each recording site, identified by a microdrive reading, to be located on the CO and 2dg images.

RESULTS

Over the course of 21 microelectrode penetrations (10 oblique, 11 perpendicular) in 18 monkeys, data were recorded from 384 different cortical sites. A single unit was isolated at 288 sites (75%); multi-unit activity was recorded at the remaining 96 sites (25%). Due to time constraints or technical problems, such as losing isolation of the neuron, quantitative data were not recorded at every site. A total of 201 area summation tests and 169 surround direction tests were performed.

Center-surround interactions

A variety of center-surround interactions were encountered (Fig. 2), but these could be categorized into two major groups. This was indicated by strong statistical evidence for a bimodal distribution of our quantitative measures of center-surround

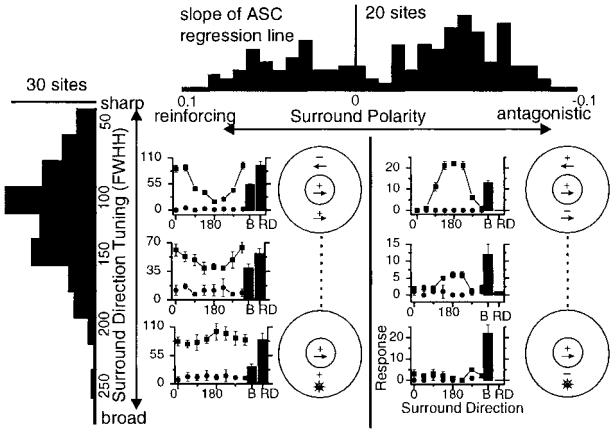

FIG. 2. Summary of receptive field types encountered. Surrounds could be either antagonistic or reinforcing with respect to the preferred direction of the center. In addition, the sharpness of direction tuning in the surround varied as well as its ability to both "push" and "pull" the response. A surround direction tuning curve is shown for each type of receptive field. On each of these plots, the pair of bars at the right depict the neuron's response to 2 control conditions: B, stimulation of the receptive field center alone using a single bar (surround dots on, but stationary); RD, stimulation of the surround alone using an annular window of random dots moving in the preferred direction of the center (center bar stationary). The line plots to the *left* represent the neuron's mean response (± SE) to various directions of surround motion in combination with the preferred direction of motion in the center. Numbers on the *x* axis are *relative* surround directions: 0 indicates surround motion in the same direction as the center (i.e., preferred direction) and 180 indicates surround motion in the direction opposite to that of the center (i.e., null direction). ■, the response when the stimulus was on and moving; ●, the level of spontaneous activity. The bar plots *above* and to the *left* are frequency distributions of parameters measured from area summation tests and surround direction tests, respectively. The *top plot* is a histogram of the slope of the regression line fit to each area summation curve (ASC). The histogram at the *left* is the width of the surround's direction tuning curve [full width at half height (FWHH) in degrees].

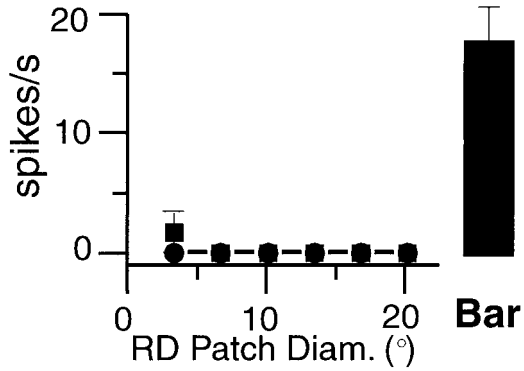

FIG. 3. Responses of a typical "bar" cell. The neuron responded poorly to all random dot stimuli, regardless of the patch size, but gave a good response to a single bar swept across the center of its receptive field.

interaction (Fig. 2, *top*), such as the slope of the regression line fit to ASC data (Shapiro-Wilk W test, $W = 0.923$, $P < 0.0001$) and the SI ($W = 0.908$, $P < 0.0001$). One group was characterized by surrounds that were directionally *antagonistic* to the center. Because of this property, none of these neurons responded well to WF motion regardless of the direction, speed, or binocular disparity of the stimulus. Within this group of local motion processing neurons, there was a continuous range of selectivity of the surround for direction. At one extreme were neurons that responded most vigorously when a centrally placed bar or small random dot patch was surrounded by an annulus of random dots moving in the *opposite* direction, as first described by Allman and colleagues (1985a). On the two quantitative tests, this receptive field type was usually characterized by an ASC that fell off dramatically as the random dot patch size increased, and, on the surround direction test, a rather sharply tuned surround that was able to both "push" and "pull" the response with respect to the center alone. This latter property is illustrated Fig. 2, *top right.* The neuron gave a good response to a single bar swept across the center of its receptive field (bar plot labeled "B"), gave no response to an annulus of random dots, showed strong suppression of the bar response when the dots in the annulus moved in the *same* direction as the center bar (0°), and showed strong facilitation when the surround dots moved in the *opposite* direction (180°). This type of push-pull behavior occurred in just under a third of the neurons that had antagonistic surrounds. For another third (Fig. 2, *middle right*), the surround was clearly direction-selective but showed *only* antagonistic effects with the suppression being minimal when the surround moved in the opposite direction to that of the center. The remaining third of the neurons with antagonistic surrounds showed suppression of the center response by surround motion in *any* direction (Fig. 2, *bottom right*).

Another characteristic of the group of cells with antagonistic surrounds was the tendency for discrete objects, such as bars or spots, to be much better stimuli than textures, such as gratings or random dots. This can be seen by comparing the ASC with the surround direction curve for the neuron in Fig. 3. The neuron responded poorly to random dot patches of any size, yet a single bar swept across the center of the receptive field (RF) gave a vigorous response. This was true of the population in general: there was a strong relationship between the qualitative rating of neurons as dot or bar cells and the absence or presence of antagonistic surrounds, respectively (χ^2 test, $P < 0.0001$).

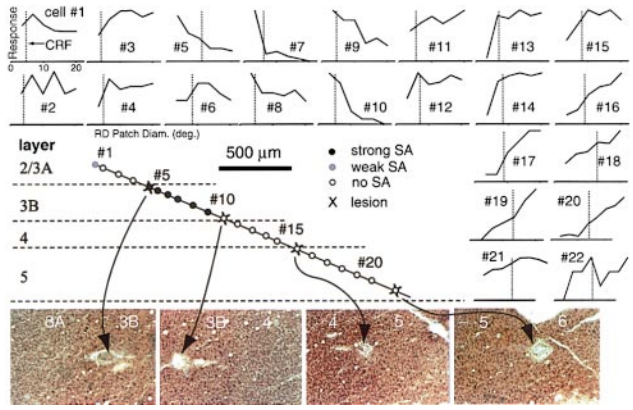

FIG. 4. Reconstruction of an oblique microelectrode penetration through the middle temporal visual area (MT). The location of each neuron encountered is depicted along with the histological sections (color panels) containing the 4 lesions produced during the penetration. Even though the sections are cut roughly parallel to the cortical surface, laminar transitions can be seen within each section. Graphs plotted around the periphery are ASCs for each neuron. In each graph, the *x* axis represents the diameter of a window of random dots moving in the neuron's preferred direction; the scale is the same for each neuron. The *y* axis is the normalized response of the cell. The dashed vertical line on each plot represents the diameter of the classical receptive field (CRF).

The other major group of neurons responded best to WF motion. In many cases, the region of increasing response, as measured by the ASC, greatly exceeded the area mapped using a single bar. This difference may have been a matter of threshold, since a response could usually be elicited by using an annulus of random dots that completely excluded the CRF. Such behavior would indicate that these regions are perhaps more properly thought of as an extension of the center rather than as a surround proper. Nevertheless it was true that excitatory regions beyond the CRF were most frequently observed in neurons outside of the input layers: compare, for example, the ASCs of *neurons 12–15* of Fig. 4, recorded from layer 4, with those from *neurons 16–20*, which were recorded from layer 5. This finding makes it likely that these regions represent the result of further processing within MT, and it remains possible that further study may reveal other differences between them and the CRF. Thus the excitatory regions beyond the CRF will henceforth be referred to as reinforcing *surrounds*.

Anatomical organization

In an earlier report (Born and Tootell 1992), we demonstrated that the qualitatively determined center-surround properties were clustered along oblique microelectrode penetrations, appeared to correspond to the 2dg band-interband patterns, and were similar along perpendicular penetrations. In the following paragraphs, the quantitative aspects of this anatomical organization will be explored in greater detail.

Figure 4 shows the results of a single, oblique penetration spanning 2 mm of the cortex. Surrounding the penetration are the ASCs for all 22 units recorded at approximately 100-μm intervals. Examining these curves reveals several clusters sharing common shapes, indicative of similar types of center-surround interactions: *units 1–4* show a general lack of surround suppression, *units 5–10* all show significant surround suppression, *units 11–14*, all recorded in layer 4, show very little influence of the regions beyond the CRF (whose boundaries are indicated by the vertical, dotted lines), and *units 16–22* show evidence for significant facilitation beyond the CRF. While the transitions in this penetration appear quite abrupt, it was not unusual to find "transitional" ASCs that showed only weak surround suppression between regions of strong suppression and facilitation.

The quantitative evidence for clustering of center-surround interactions across all penetrations was examined by the method previously used to analyze the organization of binocular disparity in the cat (LeVay and Voigt 1988) and macaque monkey (DeAngelis and Newsome 1999). For each pair of recording sites within a given penetration, the absolute value of the difference in the SI ($|\Delta SI|$) is plotted as a function of the distance between the recording sites (Fig. 5). In most cases, the single units were not sampled at precisely regular intervals so the distances were first grouped either to the nearest 200 μm (Fig. 5*A*) or, for examining longer-range interactions, to the nearest 300 μm (Fig. 5*B*). If there exists an overall organization for the measured index, then recordings from nearby locations should show smaller differences than recordings from distant locations.

This relationship is precisely what was found. For oblique penetrations (●), the difference values approach and then exceed the difference value that would be expected by chance (the average $|\Delta SI|$ obtained by randomly selecting 10,000 pairs of recording sites from the entire data set). The strong similarity between recording sites separated by distances of 2.1–2.4

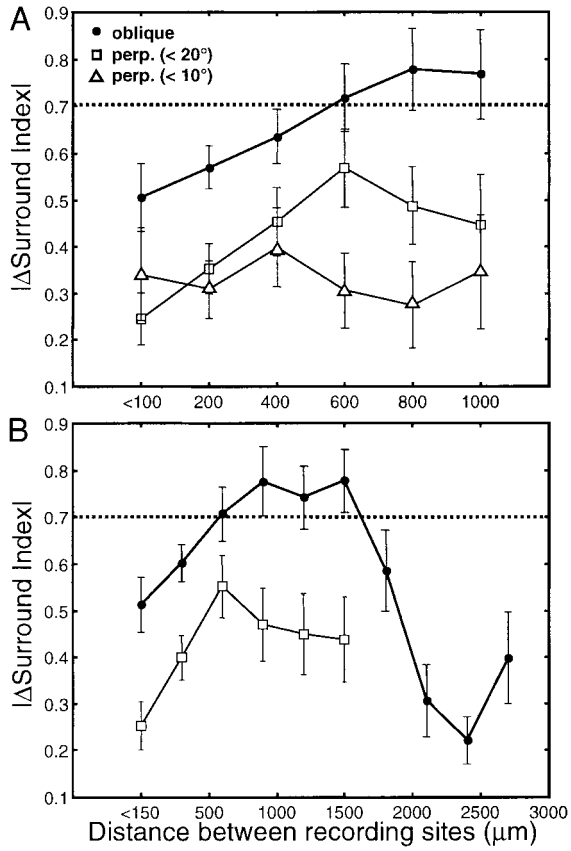

FIG. 5. Difference in center-surround interactions as a function of the distance between recording sites. ●, data from oblique penetrations; □ and △ data from perpendicular penetrations. Error bars represent the standard error of the mean. - - -, the mean difference that would be expected by chance.

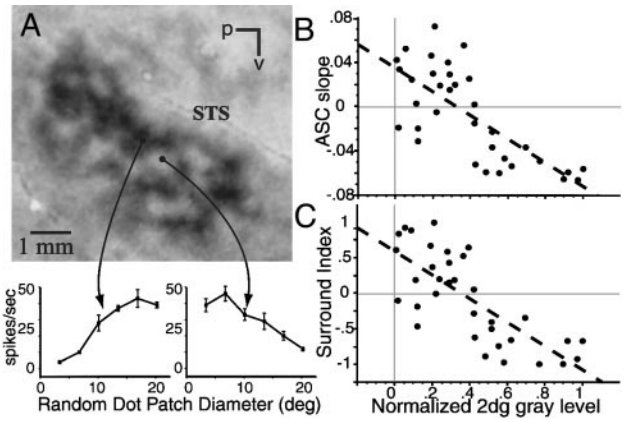

FIG. 6. Correlation of 2-deoxyglucose (2dg) labeling and neuronal receptive field properties. This figure includes all 34 neurons for which quantitative area summation data and quantitative 2dg data were obtained. *A*: 2dg labeling of the wide-field/local architecture of MT along with 2 representative ASCs from each region. Scale bar, 1 mm. *B* and *C*: quantitative responses of 34 MT neurons in the area summation test regressed against the 2dg gray-level. Two different measures of center-surround interactions were used. *B*: slope of the regression line of the ASC. *C*: surround index.

mm (Fig. 5*B*) is consistent with the band-like periodicity suggested by the 2dg patterns (Figs. 6 and 7). The difference values for perpendicular penetrations (□) were always smaller than the corresponding oblique values, consistent with an overall columnar organization. A similar picture was obtained for both oblique and perpendicular penetrations when the slope of the ASC was used as the measure of center-surround interactions.

To further examine the effects of penetration angle and distance between recording sites, a two-way ANOVA was performed. For both dependent measures (|ΔSI| and |ΔASC slope|) and for both site distance groupings (200 or 300 μm), the two main effects were highly significant ($P < 0.01$). However, in no case was the interaction term between site distance and penetration angle statistically significant ($P > 0.5$), consistent with the observed similarity in slopes between the plots for oblique and perpendicular penetrations.

This analysis of the perpendicular penetrations revealed a somewhat greater intracolumnar variability than expected. Although the difference values between recording sites within a column were always less than would be predicted by chance and always smaller than those for oblique penetrations, they nevertheless rose quite steeply with site distance over the first 0.5 mm (Fig. 5*A*, □). This may reflect a relatively weak columnar organization but might also be explained by variability in the angle of the penetration. To see if the latter was the case, the analysis was re-run using only those perpendicular penetrations (6 of 11) in which the electrode track made an angle of less than 10° with respect to the radial fibers. When this was done (Fig. 5*A*, △), the slope of the line became much flatter, and this was reflected by a significant interaction term in the two-way ANOVA ($P < 0.05$).

Thus overall this analysis provides a picture of a local columnar organization with a tendency toward periodicity at a wavelength of approximately 2 mm. This repeat distance is somewhat longer than the periodicity observed in the 2dg patterns but can be explained by two factors. First, the oblique penetrations were not perfectly parallel to the cortical surface and second, the consistent direction of the electrode penetrations, from posterior to anterior, was not strictly perpendicular to the long axis of the 2dg bands, which tend to arc around and run nearly parallel with the STS (see Figs. 6 and 7).

That the 2dg band-interband patterns reflect the clustering of neurons with similar center-surround properties was confirmed by a direct correlation of the two measures (Fig. 6). This was done for four oblique penetrations in four different animals after which a 2dg experiment was performed. For each penetration, the electrode track was superimposed on the 2dg autoradiograph, and the gray-level value underlying each recording site was determined. To permit comparisons between animals, each gray level value was normalized to the range of values found within MT for that animal. The results of this analysis show that for both the SI and ASC slope, the correlation was highly significant (SI: $r^2 = 0.565$, $P < 0.0001$; ASC slope: $r^2 = 0.534$, $P < 0.0001$) and in the expected direction: neurons whose RFs had strongly antagonistic surrounds were located in the *lightest* regions of the 2dg autoradiographs (light indicating low 2dg uptake to the WF motion stimulus) and vice versa.

Finally, additional evidence that the overall organization is columnar comes from the laminar consistency of the 2dg patterns themselves (Fig. 7). A comparison of the four panels in this figure shows the same basic features extending from the most superficial to the deepest layers. As is typical for 2dg patterns, they tend to be sharper and of higher contrast in the middle layers and more diffuse in the deep layers (Geesaman et al. 1997; Tootell and Hamilton 1989; Tootell et al. 1988). Typically the highest contrast patterns were seen in the lower part of layer 3 (Fig. 7*B*). No apparent narrowing of the 2dg columns was observed in layer 4, even though this layer, along with the very thin uppermost part of layer 6 (both of which receive inputs from V1), were most frequently the locus of discrepancies in the columnar consistency of center-surround properties (Fig. 8). The discrepancies were determined by comparing the sign of the SI of each unit with the prevailing sign for the penetration as a whole. It is noteworthy, however, that in layer 4, the discrepant units accounted for less than a quarter of the total recorded there. While discrepancies were

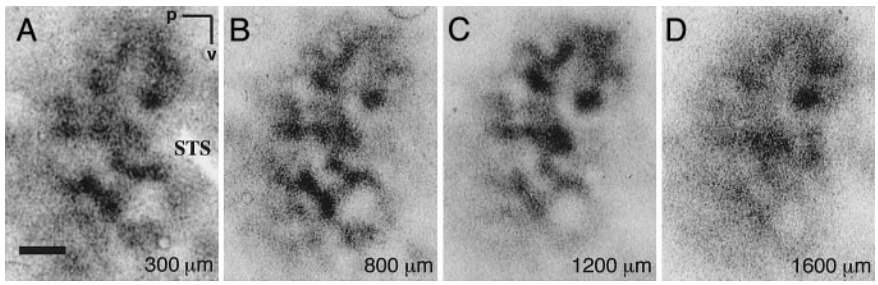

FIG. 7. 2dg patterns of tangential sections from cortical layers. Each panel is the average of 3 consecutive images centered around the depth indicated in the *bottom right* corner of the panel. The panels are from different cortical layers: 2/3A (*A*), 3B (*B*), 5 (*C*), and 6 (*D*). STS, superior temporal sulcus; V, ventral; P, posterior. Scale bar, 1 mm.

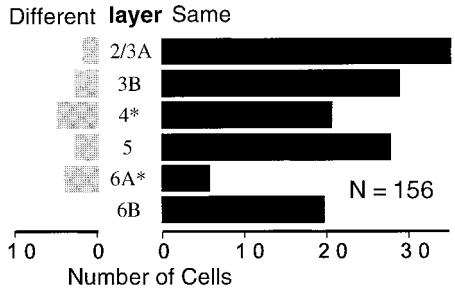

FIG. 8. Intracolumnar discrepancies as a function of layer. Each neuron was classified according to whether the sign of its interaction type (SI) was the same as or different from the type prevailing during the penetration. There were very few exceptions to the columnar pattern, and the majority of these occurred in the input layers (*).

more frequent in layer 6A (nearly 50%), this layer is probably too thin to be resolved in any of the 2dg sections (each 40-μm thick). It may account, however, for some of the decrease in contrast seen in the lower layers (Fig. 7*D*).

Relationship between center and surround

The surround direction test was used to compare the preferred directions of the center and surround. Occasionally neurons were encountered whose optimal stimulus consisted of a surround moving perpendicular to the center (shearing type motion); however, the strong overall tendency was for the surround to be maximally excitatory when it was moving in either the *same* or the *opposite* direction to that of the center (Fig. 9*A*). From the Gaussian fit to the surround direction tuning curve, a measure of the sharpness of direction tuning for the surround (Fig. 9*B*) was also obtained. Quantitative direction tuning for the centers was performed on only a subset of these neurons (Fig. 9*C*), but it was quite clear that the centers were more sharply tuned for direction than were the surrounds (mean tuning bandwidth of center = 105°; surrounds = 127°; $P = 0.0034$, Mann-Whitney U test).

On a subset of neurons, tests were performed to look for interactions between the tuning of centers and surrounds for both speed (Fig. 10) and direction (Fig. 11). These tests consisted of multiple measurements of the tuning of the center in the presence of surrounds moving at different speeds or in different directions. All of the different combinations of center and surround motion were randomly interleaved in one large block of trials. The results for relative speed tuning of a single neuron are shown in Fig. 10*C*. The preferred speed of the center was approximately 4°/s, regardless of the speed with which the surround moved. The overall responsiveness of the neuron was, however, modulated by the surround motion. This was true for the nine neurons tested quantitatively (Fig. 10*E*)—the shifts of the peak of the speed tuning curve induced by surround motion were clustered around zero, suggesting independent speed tuning for center and surround. For the pooled data, neither the slope nor the y-intercept of the regression line was significantly different from 0 ($P > 0.10$). An analogous set of measurements was made for direction tuning (Fig. 11). The results were similar in that the peak of the direction tuning curve was not shifted significantly by changes in the direction of the surround although the overall level of responsiveness was modulated by surrounds of different directions (Fig. 11*C*). This basic result was true for the three neurons tested quantitatively (Fig. 11*E*), and it was obvious for a much larger number of cells tested qualitatively.

Complex motion contrast

A subset of neurons in the interbands had RFs that could not be described as simply center-surround. Like nearly all interband cells, they responded best to bars or to small fields of random dots. They differed, however, in that an optimally sized random dot patch elicited a strong response over a rather large area of the visual field. This first became evident when the size of the CRF was superimposed on the ASC (Figs. 12*A* and 13). For such neurons the optimal random dot patch diameter was actually much *smaller* than the CRF. The optimally sized random dot patch (~1.5° in the example of Fig. 12*B*) could elicit an excitatory response over a much larger region of the visual field (approximately 4 × 4°). Note, however, that if this 4 × 4° region of the visual field was covered

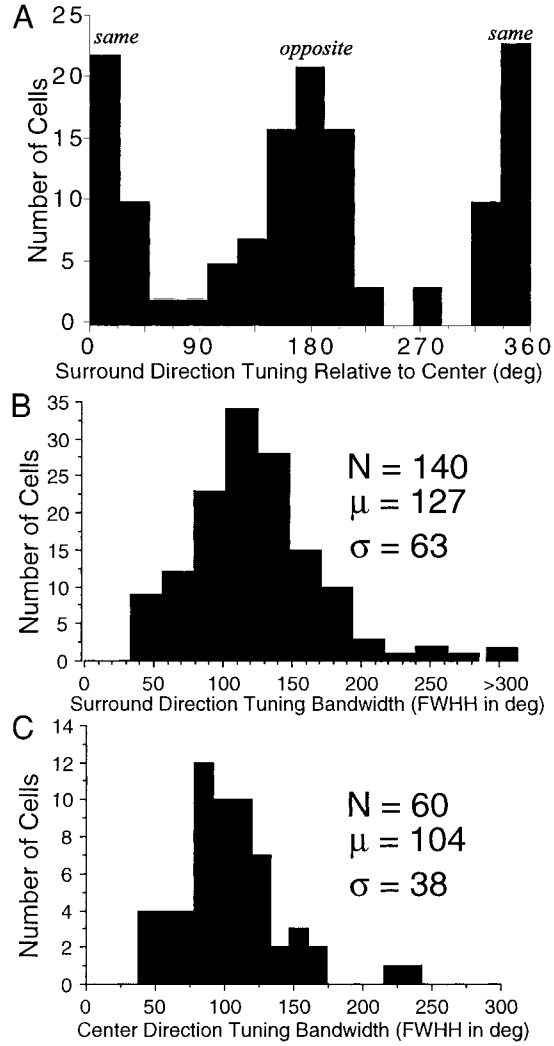

FIG. 9. Relationships between centers and surrounds. *A*: the preferred direction of the surround with respect to that of the center is plotted: a direction of 0° means that the preferred direction of the surround was the *same* as that of the center, and a direction of 180° means that it was *opposite*. *B* and *C*: the width of direction tuning for the receptive field surrounds (*A*) and centers (*B*) is expressed as FWHH and was determined from the standard deviation of a Gaussian fit to the raw data.

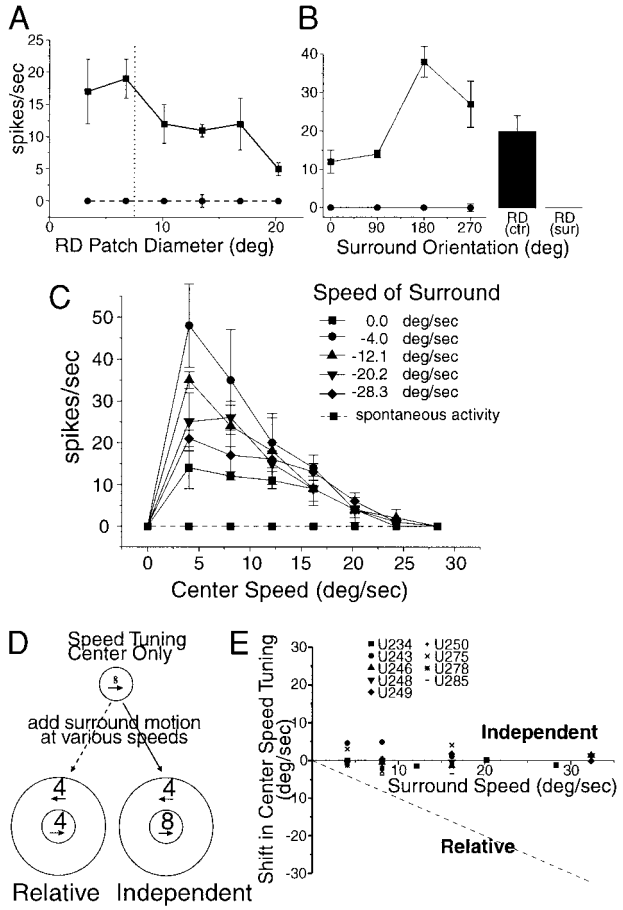

FIG. 10. Center-surround relationships for speed tuning. *A–C*: single unit recorded in layer 3B of an interband. The basic center-surround properties are shown by the area response test (*A*) and surround direction test (*B*). *C*: multiple speed tuning curves for the center while the surround was moved at various speeds always in the direction opposite to that of the center. *D*: the results predicted by 2 different hypotheses for center-surround interactions are shown schematically. If the center and surround were encoding relative speed, as the surround was moved in the opposite direction at increasing speeds, the preferred speed of the center would shift to slower speeds. Independent tuning would yield no shifts in the speed tuning of the center. *E*: results of tests on 9 neurons. For each tuning curve, the peak was determined by fitting a smoothing spline to the data ($\rho = 1.0$; each data point's contribution to the fit was weighted by its SD) and determining the x value of the highest point on the spline. The peak value for the control condition (no surround motion) was subtracted from the peak value for each curve to get a value for the shift induced by surround motion at a given speed. The quantitative predictions of the 2 hypotheses are shown on the graph of the data. The points are clustered around the x axis as predicted by the independent tuning hypothesis. For the pooled data, neither the slope nor the y intercept of the regression line was significantly different from 0 ($P > 0.05$).

with an equal-sized patch of random dots, the neuron's response was barely above baseline (Fig. 12*A*). RFs of this type appear to generalize the property of surround antagonism—or motion contrast—across retinotopic space. Because this process seems analogous to the operation performed by complex cells with respect to orientation (Hubel and Wiesel 1962) and by complex unoriented cells with respect to chromatic opponency (Hubel and Livingstone 1985), this property was termed "complex."

Once the existence of the complex RF was clear, it was found in 24 single units of 140 sites mapped (17%). The ASCs, along with the border of the CRF, are shown for a randomly chosen subset of nine of these in Fig. 13. It was obviously important to document this property for *single* units because a multi-unit response of this type might only indicate a group of neurons with simple center-surround antagonism but slightly offset RFs. Although the incidence of complex motion contrast seems rather low, neurons exhibiting it also tended to cluster, not only columnarly, within interbands, but within specific layers as well (Fig. 14). In this penetration six single units (marked by *) had RFs of the complex motion contrast type: three in layer 3B (the lowermost part of supragranular cortex containing distinctive large pyramidal neurons) and three in layer 5. Of the 24 complex motion contrast neurons, 14 were recorded in layer 3B, 10 were recorded in layer 5, and none were outside of these two layers. These facts combine to make for local densities that may be quite high. Of the 140 sites referred to above, approximately half were in bands and another quarter were outside of layers 3B and 5. If only neurons in interbands within layers 3B and 5 were considered, then complex motion contrast cells accounted for 24 of 42 (57%) of the recordings.

DISCUSSION

A survey of center-surround interactions within the RFs of neurons in owl monkey MT revealed two basic categories:

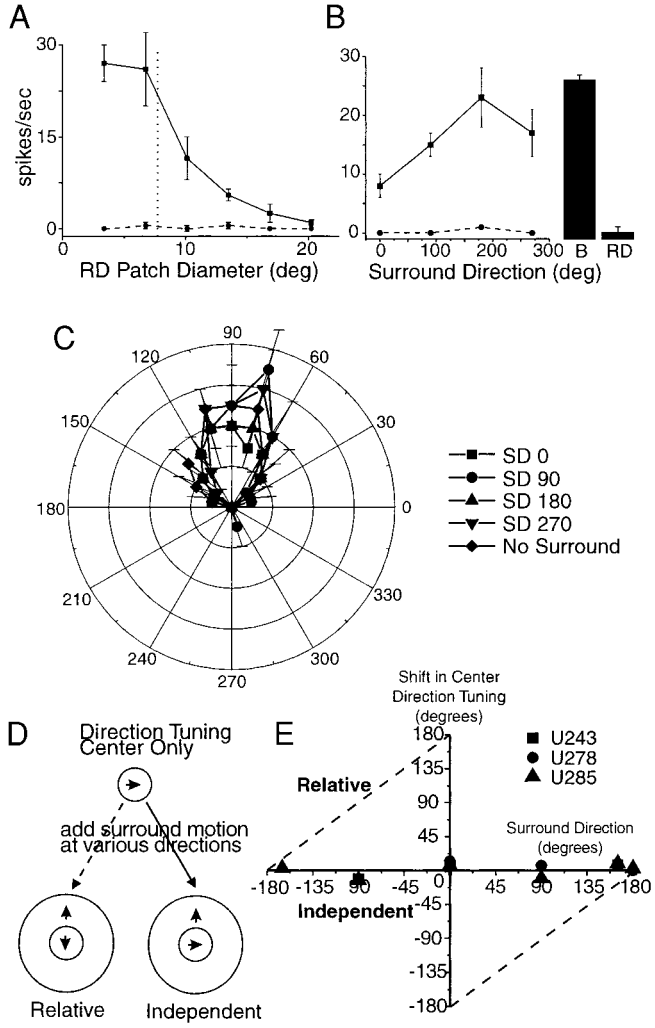

FIG. 11. Center-surround relationships for speed tuning. The format is the same as for Fig. 10.

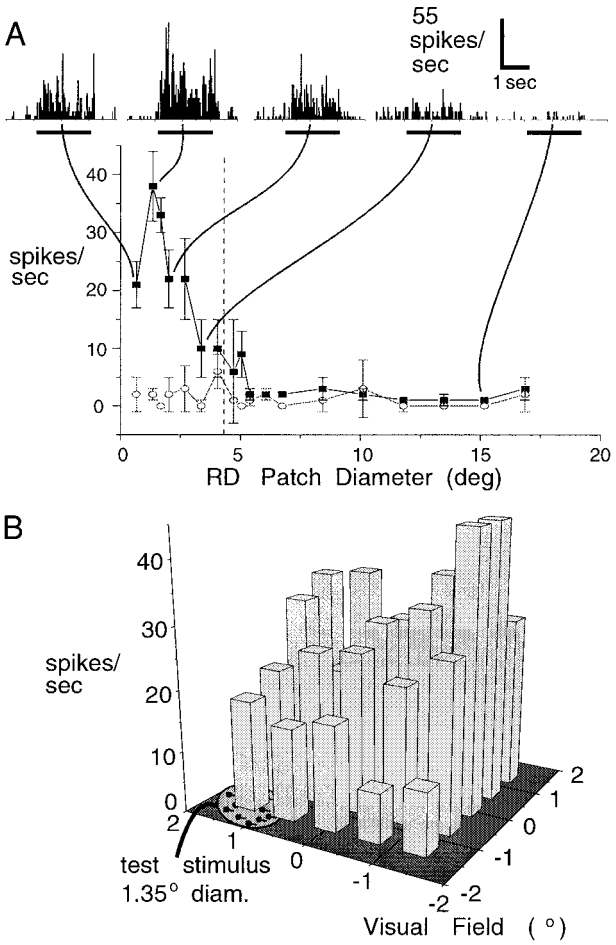

FIG. 12. Complex motion contrast. *A*: the area summation test for a neuron recorded in layer 3B of an interband. This test indicates that the optimum random dot patch was 1.35° in diameter. The diameter of the CRF is indicated by the dashed vertical line. At the *top*, peristimulus time histograms (PSTH) are shown for selected points on the curve. The dark, horizontal bar under each PSTH indicates the time during which the stimulus was on. *B*: responses of the same neuron tested with an optimally sized random dot patch at different locations within its receptive field. The neuron gives a good response over a region of the visual field which is much larger than the optimal stimulus size.

neurons with antagonistic surrounds that responded optimally to discrete objects, such as bars, and were insensitive to wide-field motion and neurons with reinforcing surrounds that responded best to wide-field motion of textures. These types were clustered together and organized anatomically into columnar slabs that could be observed directly as dark *bands* and light *interbands*, using 2dg functional labeling. For individual neurons, the preferred direction for the surrounds, with respect to that of the centers, tended to be in either the same or the opposite direction, and the direction tuning of the surrounds was broader, on average, than that of the centers. The general effect of the surrounds was not to shift the tuning of the center for either direction or speed but rather to modulate the overall responsiveness of the neuron. Finally, a RF that generalized the property of surround antagonism over retinotopic space, named "complex motion contrast," was found in layers 3B and 5 of the interbands.

Functional organization for what?

The sine qua non of MT neurons with antagonistic surrounds is that they do not respond to wide-field motion. Thus it is

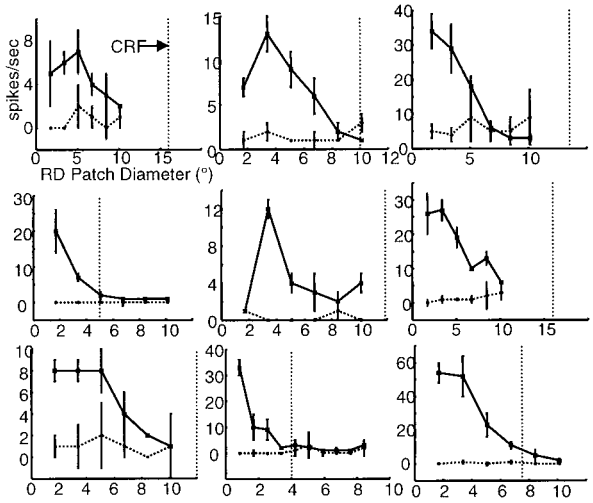

FIG. 13. ASCs for 9 neurons whose receptive fields were classified as "complex motion contrast." In each case, the peak response was to a stimulus much smaller than the width of the CRF (vertical dotted line).

plausible that the clustering of center-surround properties would produce the band-interband patterns observed in the 2dg experiments. Another possible explanation for these patterns, however, is an organization for binocular disparity such as that described in the macaque (DeAngelis and Newsome 1999). This organization consists of columnar clusters of neurons that are nonselective for binocular disparity interdigitated with zones containing systematic maps of columns of neurons preferring different disparities. Given such an organization, a wide-field motion stimulus might also produce patchy, columnar 2dg uptake, because the nonselective zones would be more

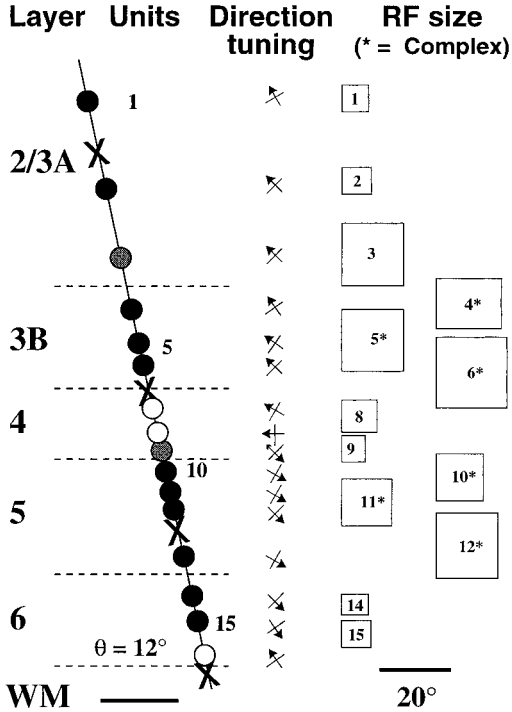

FIG. 14. A near-perpendicular penetration through an interband during which a number of complex motion contrast cells were encountered. This penetration was typical in that cells with complex receptive fields were found predominantly in the lower part of layer 3 and the upper part of layer 5. Scale bar, 200 μm.

active than those selective for a particular disparity. Even the experiments during which binocular disparity was varied over the course of the 2dg infusion would not rule out the contribution of such an organization because any given neuron within the disparity-selective zones would still be active a smaller percentage of the time. Based on the present results, however, it appears unlikely that a similar organization for binocular disparity exists in the owl monkey: neurons were always tested for sensitivity to binocular disparity, albeit qualitatively, and selectivity was only rarely found. For disparity-selective neurons, the stimulus was always presented at the optimal center disparity when performing tests of center-surround interactions. Thus differences in disparity tuning cannot account for the 2dg results in the owl monkey.

Another point worth noting is that it was difficult to find a single quantifiable parameter that adequately captured the functional organization. The ASC provided a good measure for some neurons, but it was not useful for neurons that did not respond to random dots at all (see Fig. 3). These "bar" cells were encountered very frequently within the interbands. Although an antagonistic surround could usually be demonstrated by stimulating the CRF with a bar while stimulating the surround with an annulus of random dots, it was difficult to compare this test with the ASC data. This feature undoubtedly diluted the statistical analysis of periodic organization; however, it actually strengthens the argument that the interbands are more specialized for processing object-based motion (see following text). Thus there appear to be at least two properties that distinguish the different regions labeled by 2dg: a change in the nature of the center-surround interactions, from reinforcing to antagonistic, and a change in the nature of the optimal stimulus, from more texture-like to more object-like.

Further support for the functional segregation reported here comes from a recent anatomical study where it was found that the connections of MT neurons are also segregated (Berezovskii and Born 2000). When retrograde tracers were injected into the dorsal subregion of the fundus of the superior temporal sulcus (FSTd) and MST, the labeled neurons in MT were generally restricted to either the bands or the interbands. This result both strengthens the idea that they represent different functional compartments and suggests that the distinction between wide-field and local motion processing continues at subsequent cortical stages. The previously demonstrated physiological grouping of neurons responding preferentially to local or wide-field motion in macaque area MST (Eifuku and Wurtz 1998; Komatsu and Wurtz 1988; Tanaka et al. 1986) indicates that a similar pattern may occur in old world monkeys as well.

Model of owl monkey MT

These observations on the grouping of motion-processing neurons whose RFs possess different types of spatial interactions, combined with the previously described organization for preferred direction (Malonek et al. 1994), suggest a modular organization of owl monkey MT analogous to that proposed for macaque striate cortex by Hubel and Wiesel (1977). In this model (Fig. 15), direction columns occupy one dimension and occur at a spatial scale similar to that of orientation columns in striate cortex. The band-interband organization, comprising a second dimension, is rather coarser, similar to that for ocular dominance columns in striate cortex. The purpose in putting forth such a geometrically simple model is not to suggest that these two stimulus dimensions are represented at right angles in the cortex. The actual geometry is undoubtedly more complex—again, by analogy with the relationships observed in striate cortex (Blasdel 1992; Obermayer and Blasdel 1993)—and may be more correctly described as a "polymap" than as strictly "modular" (Swindale 1990). The model merely serves to emphasize that both representations are relatively orderly and columnar, that they occur at different spatial scales, and that they are presumably not strictly parallel, since this would lead to coverage problems.

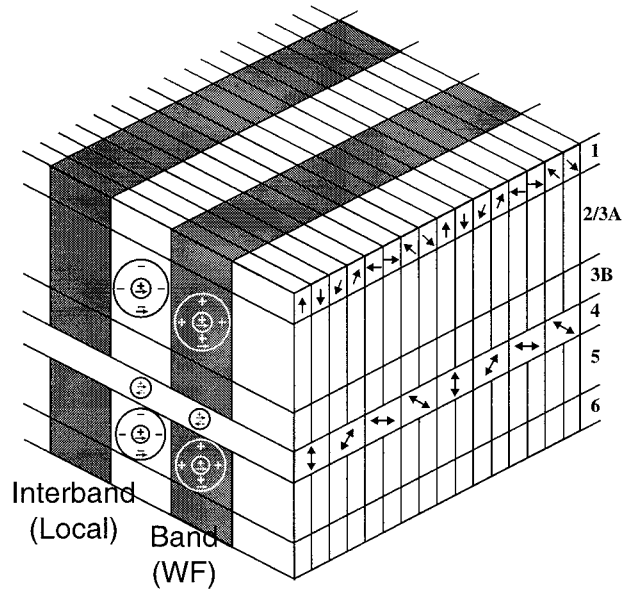

FIG. 15. A model of the functional architecture of owl monkey MT. The organization of center-surround interactions coexists with the previously described organization for direction selectivity (Malonek et al. 1994). The band-interband organization is at a coarser spatial scale than that of direction slabs, analogous to the relationship between ocular dominance and orientation slabs in striate cortex of the macaque (Hubel and Wiesel 1977).

Functional implications

Motion of images on the retina can occur either because something in the world is moving or because the retina is moving (due to eye, head, or body motion on the part of the observer). Because both types of motion usually occur together, disambiguating them is a difficult and important task for the motion system—important because they convey different kinds of information and generally call for different motor responses on the part of the animal. This has been shown most clearly in the visual system of the fly, which also appears to anatomically segregate wide-field and local-contrast motion processing neurons (Egelhaaf et al. 1988). Retinal motion caused by observer motion is necessarily wide-field and largely coherent, at least at the spatial scale of MT RFs—stimulus conditions during which only the band cells are providing useful motion signals. Interband cells, on the other hand, seem best suited to convey information about objects: either actual motion of an object or motion discontinuities in the flow field created by objects at different distances from the observer as he moves through the environment (Gibson 1950). A functional clustering of these different signals would seem to make sense,

then, since they are qualitatively different in their meaning to the organism.

Recent microstimulation experiments in macaque MT support this notion of a functional dichotomy (Born et al. 2000). Different physiologically identified regions of MT were stimulated while the monkeys performed a step-ramp visual tracking task, and the directional effects on smooth pursuit eye movements were measured. When regions that were more interband-like (i.e., those preferring local motion contrast) were stimulated, effects were seen in the preferred direction of the neurons stimulated. When band-like regions (i.e., those responsive to WF motion) were stimulated, the effects tended to be in the *opposite* direction—as if the microstimulation signal was interpreted as *background* motion in the preferred direction that induced a target-associated signal in the opposite direction (Duncker 1929).

Relationship between center and surround

Detailed tests on single units revealed that the center and surround behaved quite independently. Changes in the speed or direction of the surround did not induce shifts in the tuning of the center as one might expect if only *relative* velocity were being represented (Frost and Nakayama 1983). This does not mean, however, that relative velocity information cannot be extracted from the signals of interband neurons. Modeling studies have shown that an overall modulation of the type described here can be used to compute a truly relative signal. For example, the eye-position modulation of the retinotopic responses of neurons in posterior parietal cortex (Andersen et al. 1985, 1987) can be readily converted to a craniocentric representation of the visual world (Zipser and Andersen 1988). It seems entirely plausible that the sort of surround-modulated responses reported here might be similarly transformed to provide the true relative velocity of an object with respect to the visual background.

Complex motion contrast

The RFs of a subset of neurons in the interbands extend the property of motion surround antagonism over a larger region of the visual field. This type of RF has not been described previously in MT of either the owl monkey or the macaque, although something very similar has been described in macaque MSTl (Tanaka et al. 1986), in neurons classified as "figure type." Once sought out, this RF type proved to be quite common in owl monkey MT, and the neurons embodying it showed a high degree of topographic and laminar specificity.

The basic operation at the heart of complex motion contrast—that of taking a RF property and generalizing it over retinotopic space—appears to be quite prevalent. It has been reported in a number of other cell types, processing different visual modalities, recorded in different regions of the visual cortex: "complex cells" in striate cortex, with respect to orientation selectivity (Hubel and Wiesel 1962); "complex unoriented cells" in V2, with respect to chromatic and spatial opponency (Hubel and Livingstone 1985); "higher order hypercomplex cells" in cat area 19 (Hubel and Wiesel 1965) and monkey V4 (Desimone and Schein 1987), with respect to end-stopping; and, quite possibly, "vector field" cells in MST, with respect to optic flow (Duffy and Wurtz 1991).

As previously suggested by Hubel and Wiesel (1962), this type of RF may be realized by a very generic type of circuit, which might be constructed by "or-gating" together inputs from many neurons with simple antagonistic surrounds for moving stimuli. Because of the surround inhibition in the input cells, the complex cell behaves more like an *exclusive* "or" gate: two small patches of motion are less effective than one, presumably because the second patch impinges on the surrounds of neurons excited by the first patch (and vice versa) thus less effectively driving any of the input cells.

Finally, the existence of the simple and complex types of motion-contrast neurons represents another example of a general tendency in hierarchical processing, first noted by Barlow (1993), to alternate RFs that are *more selective* than their predecessors along some stimulus dimension with those that are *less selective*. In this case, the simple type of antagonistic RF is more selective than previous motion processing RFs by virtue of its antagonistic surround. It responds only to motion *contrast*. The complex version, while retaining the requirement for contrast, is less selective in terms of the exact retinotopic position of the stimulus. The purpose of this alternation remains mysterious; however, its repeated appearance may indicate that the cerebral cortex is relatively computationally homogeneous. It will be interesting to see if these trends continue further along the visual pathways and whether evidence for similar kinds of circuitry will be found in higher-level association cortex as well.

I am grateful to R. Tootell for advice and support during early stages of this work. E. Kaufman provided excellent technical assistance. D. Hubel and C. Pack made helpful comments on the manuscript.

This work was supported by National Institutes of Health Grants EY-11379, EY-12196, and RR-00168 and by a grant from the Klingenstein Foundation.

REFERENCES

ALLMAN JM, MIEZIN F, AND MCGUINNESS E. Direction- and velocity-specific responses from beyond the classical receptive field in the middle temporal visual area (MT). *Perception* 14: 105–126, 1985a.

ALLMAN JM, MIEZIN F, AND MCGUINNESS E. Stimulus specific responses from beyond the classical receptive field: neurophysiological mechanisms for local-global comparisons in visual neurons. *Annu Rev Neurosci* 8: 407–430, 1985b.

ANDERSEN RA, ESSICK GK, AND SIEGEL RM. Encoding of spatial location by posterior parietal neurons. *Science* 230: 456–458, 1985.

ANDERSEN RA, ESSICK GK, AND SIEGEL RM. Neurons of area 7 activated by both visual stimuli and oculomotor behavior. *Exp Brain Res* 67: 316–322, 1987.

ATTNEAVE F. Some informational aspects of visual perception. *Psychol Rev* 61: 183–193, 1954.

BARLOW HB. Summation and inhibition in the frog's retina. *J Physiol (Lond)* 119: 69–88, 1953.

BARLOW HB. Object identification and cortical organization. In: *Functional Organization of the Human Visual Cortex* (1st. ed.), edited by Gulyas B, Ottoson D, and Roland PE. Oxford: Pergamon, 1993, p. 75–100.

BARLOW HB, BLAKEMORE C, AND PETTIGREW JD. The neural mechanism of binocular depth discrimination. *J Physiol (Lond)* 193: 327–342, 1967.

BASTIAN J. Receptive fields of cerebellar cells receiving exteroceptive input in a gymnotid fish. *J Neurophysiol* 38: 285–300, 1974.

BEREZOVSKII VK AND BORN RT. Specificity of projections from wide-field and local motion processing regions within the middle temporal visual area of the owl monkey. *J Neurosci* 20: 1157–1169, 2000.

BLASDEL GG. Orientation selectivity, preference, and continuity in monkey striate cortex. *J Neurosci* 12: 3139–3161, 1992.

BORN RT, GROH JM, ZHAO R, AND LUKASEWYCZ SL. Segregation of object and background motion in visual area MT: effects of microstimulation on eye movements. *Neuron* 26: 725–734, 2000.

BORN RT AND TOOTELL RBH. Segregation of global and local motion processing in primate middle temporal visual area. *Nature* 357: 497–499, 1992.

CARNEY T AND SHADLEN MN. Dichoptic activation of the early motion system. *Vision Res* 33: 1977–1995, 1993.

CRAIK RL, HAND PJ, AND LEVIN BE. Locus coeruleus input affects glucose metabolism in activated rat barrel cortex. *Brain Res Bull* 19: 495–499, 1987.

DEANGELIS GC AND NEWSOME WT. Organization of disparity-selective neurons in macaque area MT. *J Neurosci* 19: 1398–1415, 1999.

DESIMONE R AND SCHEIN SJ. Visual properties of neurons in area V4 of the macaque: to stimulus form. *J Neurophysiol* 57: 835–868, 1987.

DUFFY CJ AND WURTZ RH. Sensitivity of MST neurons to optic flow stimuli. II. Mechanisms of response selectivity revealed by small-field stimuli. *J Neurophysiol* 65: 1346–1359, 1991.

DUNCKER K. Über induzierte Bewegung (Ein Beitrag zur Theorie optisch wahrgenommener Bewegung). *Psychol Forsch* 12: 180–259, 1929.

EGELHAAF M, HAUSEN K, REICHARDT W, AND WEHRHAHN C. Visual course control in flies relies on neuronal computation of object and background motion. *Trends Neurosci* 11: 351–358, 1988.

EIFUKU S AND WURTZ RH. Response to motion in extrastriate area MSTl: center-surround interactions. *J Neurophysiol* 80: 282–296, 1998.

FROST BJ AND NAKAYAMA K. Single visual neurons code opposing motion independent of direction. *Science* 220: 744–745, 1983.

FROST BJ, SCILLEY PL, AND WONG SCP. Moving background patterns reveal double-opponency of directionally specific pigeon tectal neurons. *Exp Brain Res* 43: 173–185, 1981.

GEESAMAN BJ, BORN RT, ANDERSEN RA, AND TOOTELL RBH. Maps of complex motion selectivity in the superior temporal cortex of the alert macaque monkey: a double-label 2-deoxyglucose study. *Cereb Cortex* 7: 749–757, 1997.

GIBSON JJ. *The Perception of the Visual World.* Boston: Houghton Mifflin, 1950.

GROSSBERG S. The quantized geometry of visual space: the coherent computation of depth, form, and lightness. *Behav Brain Sci* 6: 625–657, 1983.

HARTLINE HK. The nerve messages in the fibers of the visual pathway. *J Opt Soc Am* 30: 239–247, 1940.

HUBEL DH AND LIVINGSTONE MS. Complex-unoriented cells in a subregion of primate area 18. *Nature* 315: 325–327, 1985.

HUBEL DH AND WIESEL TN. Receptive fields, binocular interaction and functional architecture in the cat's visual cortex. *J Physiol (Lond)* 160: 106–154, 1962.

HUBEL DH AND WIESEL TN. Receptive fields and functional architecture in two non-striate visual areas (18 and 19) of the cat. *J Neurophysiol* 28: 229–289, 1965.

HUBEL DH AND WIESEL TN. Ferrier lecture. Functional architecture of macaque monkey visual cortex. *Proc R Soc Lond B Biol Sci* 198: 1–59, 1977.

KANEKO A. Physiological and morphological identification of horizontal, bipolar, and amacrine cells in the goldfish retina. *J Physiol (Lond)* 207: 623–633, 1970.

KENNEDY C, DES ROSIERS M, JEHLE JW, REIVICH M, SHARP F, AND SOKOLOFF L. Mapping of functional neural pathways by autoradiographic survey of local metabolic rate with [^{14}C]deoxyglucose. *Science* 187: 850–853, 1975.

KNUDSEN EI AND KONISHI M. Center-surround organization of auditory receptive fields in the owl. *Science* 202: 778–780, 1978.

KOMATSU H AND WURTZ RH. Relation of cortical areas MT and MST to pursuit eye movements. I. Localization and visual properties of neurons. *J Neurophysiol* 60: 580–603, 1988.

KUFFLER SW. Discharge patterns and functional organization of mammalian retina. *J Neurophysiol* 16: 37–68, 1953.

LAGAE L, GULYAS B, RAIGUEL SE, AND ORBAN GA. Laminar analysis of motion information processing in macaque V5. *Brain Res* 496: 361–367, 1989.

LEVAY S AND VOIGT T. Ocular dominance and disparity coding in cat visual cortex. *Vis Neurosci* 1: 395–414, 1988.

MALONEK D, TOOTELL RBH, AND GRINVALD A. Optical imaging reveals the functional architecture of neurons processing shape and motion in owl monkey area MT. *Proc R Soc Lond B Biol Sci* 258: 109–119, 1994.

MATURANA HR, LETTVIN JY, MCCULLOCH WS, AND PITTS WH. Anatomy and physiology of vision in the frog (*Rana pipiens*). *J Gen Physiol* 43: 129–175, 1960.

MERRILL EG AND AINSWORTH A. Glass-coated platinum-plated tungsten microelectrodes. *Med Biol Eng* 10: 662–672, 1972.

MOUNTCASTLE VB AND POWELL TPS. Neural mechanisms subserving cutaneous sensibility with special reference to the role of afferent inhibition in sensory perception and discrimination. *Bull Johns Hopkins Hosp* 105: 201–232, 1959.

NAKAYAMA K AND LOOMIS JM. Optical velocity patterns, velocity-sensitive neurons, and space perception: a hypothesis. *Perception* 3: 63–80, 1974.

OBERMAYER K AND BLASDEL GG. Geometry of orientation and ocular dominance columns in monkey striate cortex. *J Neurosci* 13: 4114–4129, 1993.

ROCKLAND KS. Bistratified distribution of terminal arbors of individual axons projecting from area V1 to middle temporal area (MT) in the macaque monkey. *Vis Neurosci* 3: 155–170, 1989.

SCHEIN SJ AND DESIMONE R. Spectral properties of V4 neurons in the macaque. *J Neurosci* 10: 3369–3389, 1990.

STERLING P AND WICKELGREN BG. Visual receptive fields in the superior colliculus of the cat. *J Neurophysiol* 32: 1–15, 1969.

SWINDALE NV. Is the cerebral cortex modular? *Trends Neurosci* 13: 487–492, 1990.

TANAKA K, HIKOSAKA K, SAITO H, YUKIE M, FUKADA Y, AND IWAI E. Analysis of local and wide-field movements in the superior temporal visual areas of the macaque monkey. *J Neurosci* 6: 134–144, 1986.

TOOTELL RBH AND HAMILTON SL. Functional anatomy of the second visual area (V2) in the macaque. *J Neurosci* 9: 2620–2644, 1989.

TOOTELL RBH, HAMILTON SL, SILVERMAN MS, AND SWITKES E. Functional anatomy of macaque striate cortex. I. Ocular dominance, binocular interactions, and baseline conditions. *J Neurosci* 8: 1500–1530, 1988.

TOOTELL RBH AND SILVERMAN MS. Two methods for flat-mounting cortical tissue. *J Neurosci Methods* 15: 177–190, 1985.

VON GRUNAU M AND FROST BJ. Double-opponent-process mechanism underlying RF-structure of directionally specific cells of cat lateral suprasylvian visual area. *Exp Brain Res* 49: 84–92, 1983.

WERBLIN FS AND DOWLING JE. Organization of the retina of the mudpuppy, *Necturus maculosus*. *J Neurophysiol* 32: 339–355, 1969.

WONG-RILEY MT. Columnar cortico-cortical interconnections within the visual system of the squirrel and macaque monkeys. *Brain Res* 162: 201–217, 1979.

YOKOI M, MORI K, AND NAKANISHI S. Refinement of odor molecule tuning by dendrodendritic synaptic inhibition in the olfactory bulb. *Proc Natl Acad Sci USA* 92: 3371–3375, 1995.

ZIPSER D AND ANDERSEN RA. A back-propagation programmed network that simulates response properties of a subset of posterior parietal neurons. *Nature* 331: 679–684, 1988.